IEEE Access
Multidisciplinary ⋮ Rapid Review ⋮ Open Access Journal

Received 10 December 2022, accepted 30 December 2022, date of publication 3 January 2023, date of current version 6 January 2023.

Digital Object Identifier 10.1109/ACCESS.2023.3234024

RESEARCH ARTICLE

A Compact Broadband Circularly Polarized Wide-Slot Antenna With Axial Ratio Bandwidth Encompassing LTE 42 and LTE 43 Standards of 5G Mid-Band

FALIH M. ALNAHWI[1], YASIR I. A. AL-YASIR[2], (Member, IEEE), NAZAR T. ALI[3], (Senior Member, IEEE), IBRAHIM GHARBIA[2], ABDULKAREEM S. ABDULLAH[1], (Senior Member, IEEE), YIM FUN HU[2], (Senior Member, IEEE), AND RAED A. ABD-ALHAMEED[2,4], (Senior Member, IEEE)

[1]Department of Electrical Engineering, College of Engineering, University of Basrah, Basrah 61001, Iraq
[2]Bradford-Renduchintala Centre for Space AI, Faculty of Engineering and Informatics, University of Bradford, BD7 1DP Bradford, U.K.
[3]Department of Electrical Engineering and Computer Science, Khalifa University, Abu Dhabi, United Arab Emirates
[4]Department of Information and Communication Engineering, Basrah University College of Science and Technology, Basra 61004, Iraq

Corresponding author: Raed A. Abd-Alhameed (r.a.a.abd@bradford.ac.uk)

This work was supported in part by the U.K. Engineering and Physical Sciences Research Council (EPSRC) under Grant EP/E022936/1, and in part by the European Union's Horizon 2020 Research and Innovation Programme under Grant H2020-MSCA-ITN-2016 SECRET-722424.

ABSTRACT This study presents a compact broadband wide-slot antenna with broadband left-hand circular polarization compatible with both LTE 42 and LTE 43 standards of 5G mid-band applications. The proposed antenna is fabricated on an FR4 dielectric substrate with overall dimensions of $0.41\lambda_o \times 0.36\lambda_o \times 0.02\lambda_o$, where λ_o is the free space wavelength at the resonant frequency of the antenna. The antenna ground plane is etched to form a square radiating slot with a pair of rectangular ground stubs that are diagonally placed inside the slot. On the other side of the antenna, the feed line is loaded by horizontal and vertical stubs to improve the coupling between the feed line and the square slot. To generate a circular polarization, the feeding stubs cooperate with the pair of rectangular ground stubs to excite the radiating slot of the antenna at two different feeding points whose currents have approximately equal amplitude and 90° phase shift. The measured impedance bandwidth (BW) of the proposed wide-slot antenna is 16.2% (580 MHz along the band 3.3-3.88 GHz), while the observed axial ratio bandwidth (ARBW) is 12.2% (440 MHz in the 3.4-3.84 GHz band). The measured gain values are found to be larger than 2.5 dB along both standards of the 5G mid-band applications.

INDEX TERMS Axial ratio, circular polarization, wide-slot antenna, reflection coefficient, broadband.

I. INTRODUCTION

The demand for antennas with Circular Polarization (CP) increases day by day due to their unique capability in mitigating multipath fading and polarization mismatch [1], [2]. These outstanding features make the CP antennas to be a good candidate for many wireless applications such as WLAN, WiMAX, 5G, satellite, and so on. In CP antennas, it is essential to present CP that perfectly covers the intended frequency range with stable and acceptable gain value. In other words, the broadside 3dB Axial Ratio Bandwidth (ARBW), which represents the metric of the CP, should

The associate editor coordinating the review of this manuscript and approving it for publication was Tutku Karacolak.

extend along the specified frequency range of the application of interest with as small return losses as possible and as high gain as possible.

The CP antenna can be designed as a multiband antenna [3], [4], [5], in which the 3dB ARBW partially covers the intended bands. On the other hand, there is the choice of providing a wideband (or ultra-wideband) CP [6], [7], [8], [9] with −10dB impedance bandwidth (BW) and 3dB ARBW that are not specified for certain applications. The broadband CP antennas deal with providing ARBW that occupies a certain application and impedance BW that has a minimized residual effect on the adjacent frequency bands. The broadband CP antennas is the main theme of this work. In [10], a CP patch antenna is combined with a linearly polarized slot antenna to provide polarization diversity in the 5.8 GHz WLAN applications. The same band is covered with CP using 2 × 2 antenna array to present a directive CP [11]. An ARBW within the frequency range (5.53-5.63) GHz is acquired with the aid of a truncated rectangular patch and defected ground plane [12]. The design in [13] is a dielectric resonator whose ARBW extends along the range (5.2-5.58) GHz. The frequency range of the X-band satellite is covered by a CP using a dielectric resonator antenna that is fed by dual ports [14] and a leaky-wave antenna [15]. A CP frequency range of (5.4-5.7) GHz is attained with the aid of a dual patch microstrip antenna with coaxial feeding [16]. In [17], the slotted microstrip antenna with proximity-coupled feeding is utilized to generate CP for 5G mid-band applications that are used the LTE 43 standard (3.6-3.8) GHz. Unfortunately, most of the aforementioned broadband CP antennas has 3dB ARBW that partially covered the desired band, so the antenna in this work is intended to have a small size, acceptable realized gain, and perfect CP coverage for the entire band of interest.

In this paper, a compact wide-slot antenna is presented as a CP antenna whose 3dB ARBW perfectly covers the two standards of the 5G mid-band applications namely LTE 42 (3.4-3.6) GHz and LTE 43 (3.6-3.8) GHz. Although the antenna has a single feed, the shape of its slot and the feeding structure is modified to inject currents to the radiating slot at two different points with equal amplitude and 90° phase shift to generate CP at the intended bands. The simulation and measured results verify that the impedance BW of the antenna and the ARBW perfectly encompasses both standards of the 5G mid-band applications with gain values exceeding 2.5 dBi along the operational band. The rest of the paper is organized as follows. Section II presents the structure and the overall dimensions of the proposed design, whereas Section III reveals the steps that were followed to reach the final design. In Section IV, the mechanism that leads to generate CP in the broadside direction is discussed in detail. A parametric study is introduced in Section V to investigate the effect of some important parameters on the performance of the antenna. Section VI demonstrates a comparison between the simulated and measured results, while Section VII summarizes the paper with brief conclusion.

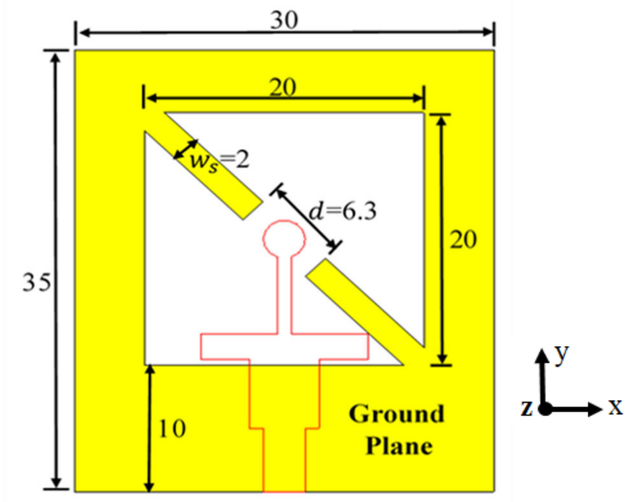

(a)

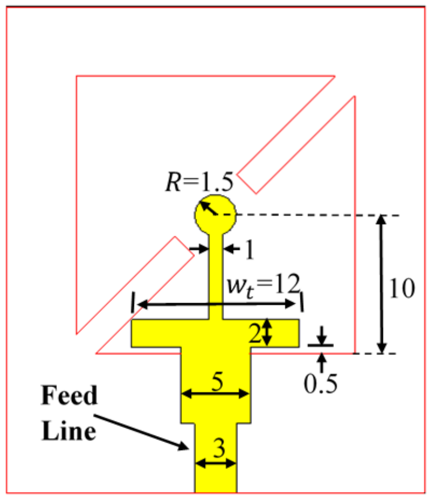

(b)

FIGURE 1. Structure of the proposed wide slot antenna (a) front view and (b) back view (all dimensions are in mm).

II. ANTENNA STRUCTURE

Since the radiation of the wide-slot antenna mainly comes from the slot that is etched on the ground plane of the antenna [18], [19], it is reasonable to illustrate the ground plane side of the antenna as a front view and the feed line side as a back view as shown in Figure 1(a) and (b), respectively. The dielectric substrate of the proposed wide-slot antenna is FR4 with a dielectric constant of $\varepsilon_r = 4.3$, height of $h = 1.6\ mm$, and loss tangent of 0.025. It is clear from the figure that the overall dimensions of the antenna are $30 \times 35 \times 1.6 mm^3$. As will be discussed in Section IV, the horizontal feeding stub whose width is equal to w_t is used to electromagnetically feed the square slot of the antenna at its lower angle. To provide another feeding point to the rectangular slot at its upper angle, the vertical feeding stub that is terminated with a circle with radius R is coupled electromagnetically with the square slot via two rectangular stubs at the ground plane both with a width of w_s separated

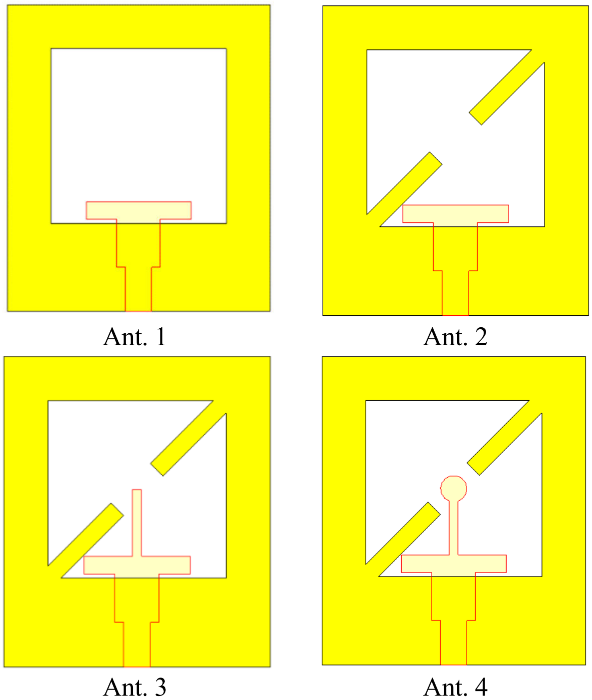

FIGURE 2. Design steps of the proposed wide-slot antenna.

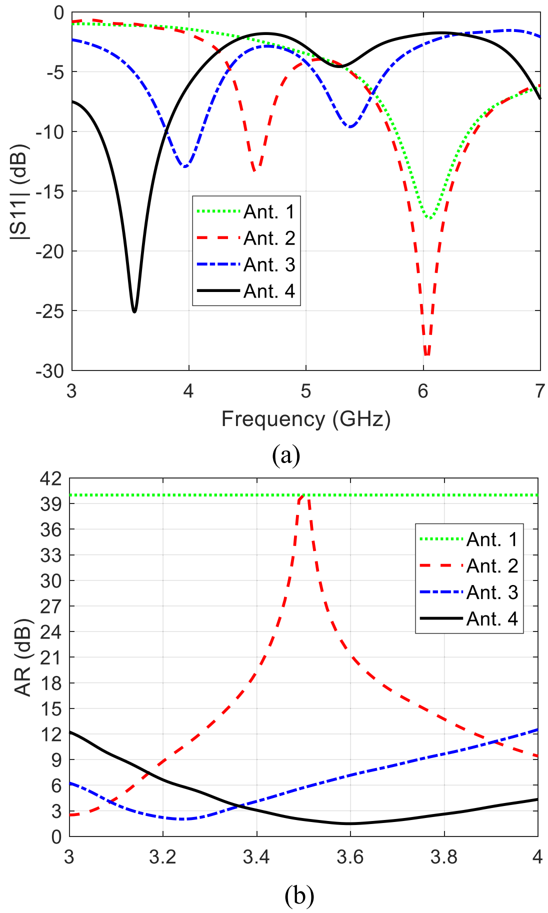

FIGURE 3. Simulation results of Ant. 1-4: (a) reflection coefficient and (b) axial ratio.

by a distance d. The feeding currents at both feeding points are intended to be with equal amplitude and 90° phase shift to generate radiation with CP.

III. DESIGN STEPS

The design procedure that was followed to reach the final scheme of the proposed antenna can be concluded in four steps (Ant.1-4) as exhibited in Figure 2, whereas the simulated reflection coefficient (S_{11}) and the broadside axial ratio (AR) corresponding to each structure are illustrated in Figure 3. It is worth to mention that the simulation results are acquired with the aid of CST microwave studio suite [20].

Ant.1 is a conventional wide-slot antenna with a rectangular radiating slot. The reflection coefficient of this step shows that the antenna resonates at 6 GHz, and the antenna broadside AR shows that the antenna is linearly polarized since there is no AR value less than 3 dB. The presence of the two rectangular stubs in Ant.2 increases the length of the electrical path of the current passing through the edge of the rectangular slot. Therefore, another resonant frequency appears at 4.6 GHz in the reflection coefficient corresponding to Ant.2. The detailed explanation of the outcomes of Ant.2 is given in [1] and [2]. The resonant wavelength that is corresponding to the antenna resonant frequency ($\lambda = c/f$) is directly proportional to the length of the current path. Therefore, the insertion of the two rectangular ground stubs provides another longer current path, which results in longer resonant wavelength whose resonant frequency is equal to 4.6 GHz in addition to the original resonant frequency of the antenna at 6 GHz. However, this variation does not contribute to presenting a CP within the matched bands since the values of the AR still larger than 3 dB within these bands. The third step (Ant.3) can be considered as a trial to provide another feeding at the upper angle of the square radiating slot by providing another electromagnetic coupling via the vertical feeding stub and the pair of rectangular ground stubs. In this step, the 3dB ARBW is improved to 200 MHz along the range (3.12-3.32) GHz.

In the final step (Ant.4), the coupling between the feed line and the square slot at the second feeding point is enhanced by terminating the vertical stub by a circular patch. This patch results in a resonant frequency equal to 3.55 GHz with broadband 3dB ARBW. The −10dB impedance BW of Ant.4 is equal to 590 MHz (16.7%) and extends along the frequency range (3.23-3.82) GHz, while the 3dB ARBW is equal to 490 MHz (13.5%) along the range (3.38-3.87) GHz. In terms of impedance BW and ARBW, it is clear that the proposed design perfectly covers the LTE 42 (3.4-3.6) GHz and LTE 43 (3.6-3.8) GHz which are utilized as two different standards for 5G mid-band applications. As a result, the proposed antenna can be used for devices that can be utilized for both standards without the need for an additional antenna.

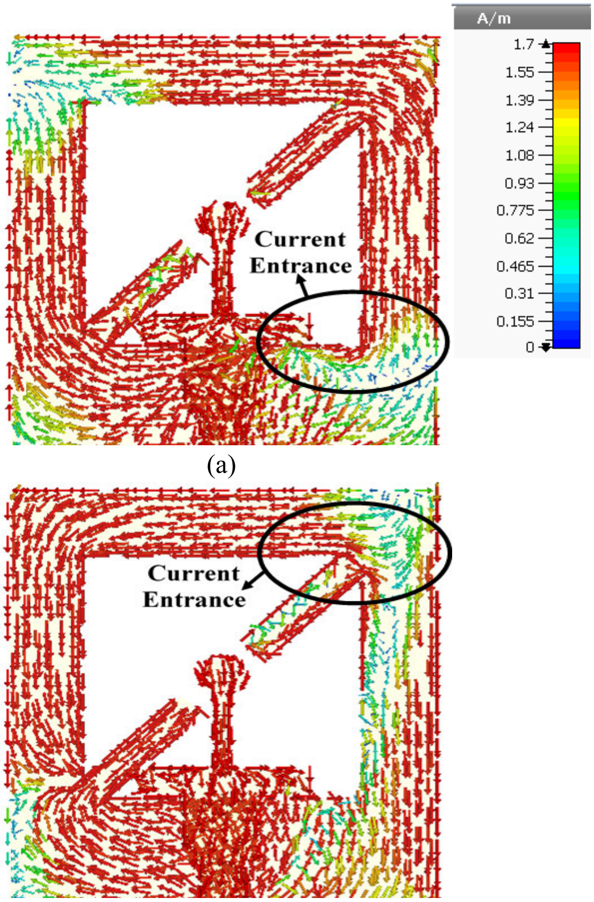

FIGURE 4. Current distributions of the proposed wide-slot antenna at (a) $\omega t = 0°$ and (b) $\omega t = 90°$ to reveal the feeding point at different instants at 3.55 GHz.

IV. MECHANISM OF THE GENERATION OF CP

As mentioned earlier, the criterion followed by this work in generating the CP is accomplished by feeding the square radiating slot of the antenna at two different locations. The structure of the feed line and the radiating slot are modified to force the currents at each point to be approximately of equal amplitudes and 90° phase shift at the resonant frequency of 3.55 GHz. Figure 4 illustrates the current distribution of the antenna at 3.55 GHz to verify the aforementioned claim. Figure 4(a) shows the current distribution at $\omega t = 0°$. At this time instant, the current flowing around the square slot approximately enters at the lower angle of the right side of the slot. In other words, the current starts to enter the square ring that holds the radiating slot at the highlighted region in Figure 4(a). On the other hand, Figure 4(b) shows the current entrance at the upper angle of the right side of the square slot when $\omega t = 90°$. This means that the current starts to enter the square ring enclosing the radiating slot at the region indicated in Figure 4(b). This demonstration gives an initial indication for the 90° phase shift between the two feeding currents, which is necessary to create CP.

To give deep insight into understanding the generation of the CP, Figure 5 depicts a schematic diagram of the current paths that feed the square radiating slot. As in [21] and [22], the two feeding points are 90° separated from each other with respect to the center of the radiating element. From Figure 5, the current is passing the lower edge of the square slot at point (A). The line segments are chosen to be compatible with the dimensions given in Figure 1. The current path of the first feeding point is passed through ($\overline{AB}$) then to ($\overline{BC}$), where $\overline{BC}$ is a hypotenuse of the triangle (ABC). Therefore, length of the first current path (Path 1) can be estimated starting from point (A):

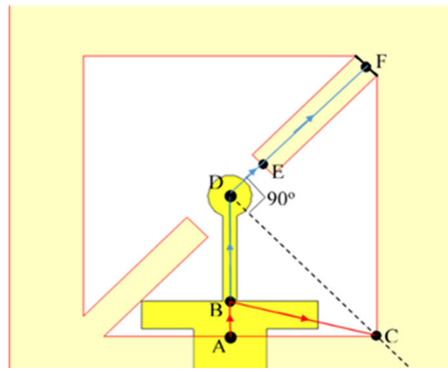

FIGURE 5. Analysis of the current path for both feeding points (C and F) of the proposed wide-slot antenna.

$$Path1 = \overline{AB} + \sqrt{\overline{AB}^2 + \overline{AC}^2} \tag{1}$$

The second current path is passed through the line segments ($\overline{AB}$), ($\overline{BD}$), ($\overline{DE}$), and ($\overline{EF}$), so the length of the second current path ($Path2$) is given as:

$$Path2 = \overline{AB} + \overline{BD} + \overline{DE} + \overline{EF} \tag{2}$$

The length of each line segment can be found from the geometry given in Figure 1 as: $\overline{AB} = 2.5\ mm$, $\overline{AC} = 10\ mm$, $\overline{BD} = 10\ mm$, $\overline{DE} = 3.15\ mm$, and $\overline{EF} = 10\ mm$. Consequently, equations (1) and (2) result in $Path1 = 12.81\ mm$ and $Path2 = 25.65\ mm$. The difference between the lengths of the paths is equal to 12.84 mm, which is approximately equal to the quarter wavelength at the resonant frequency 3.55 GHz as given below:

$$Path\ 2 - Path\ 1 \cong \frac{\lambda_g}{4} = \frac{c}{4f_o\sqrt{\frac{\varepsilon_r+1}{2}}} \tag{3}$$

where λ_g represents the guided wavelength, f_o is the resonant frequency of the antenna, c denotes the speed of light in freespace, and ε_r is the dielectric constant of the antenna substrate. By substituting the value of the resonant frequency of the proposed antenna ($f_o = 3.55\ GHz$), the quarter wavelength is found as ($\frac{\lambda_g}{4} = 12.9\ mm$), which is very close to the difference between the lengths of the two current paths. The result of equation (3) mathematically verifies the 90° phase shift between the currents of each feeding point. However, it is important to notify that the amplitudes of both currents cannot exactly be equal since the length of the paths are unequal in length, so the current of each path undergoes a different amount of losses. Therefore, the lowest value for the AR is found to be equal to 1.27.

The wide coverage of the 3dB ARBW can be explained with the aid of the 3D axial ratio patterns shown in Figure 6. It is found that the antenna has two CP regions that are not in the broadside direction as shown in Figure 6(a). At f=3.38 GHz which is the lower frequency margin of the 3dB ARBW, the two CP regions meet each other in the broad side direction (see Figure 6(b)). Within the 3dB ARBW, the two regions overlap each other in the broadside direction as illustrated in Figures 6(c) and (d). The two CP regions start to detach from each other at f=3.87 GHz which represents the higher frequency margin of the 3dB ARBW (see Figure 6(e)). Finally, Figure 6(f) shows that the two CP regions are separated from each other outside the 3dB ARBW. The ARBW has broadband coverage because it results from the overlapping of two CP regions, so losing CP in the broadside direction requires a wide range of frequencies until detaching the two regions from each other.

The direction of the rotation of the proposed antenna can be exposed using the simulated radiation pattern at 3.55 GHz shown in Figure 7. In the broadside direction ($\theta = 0°$), the left-hand circular polarization (LHCP) is dominating. To obtain right-hand CP (RHCP), the location of the rectangular ground stubs should be changed to the other diagonal of the square radiating slot.

V. PARAMETRIC STUDY

In this section, the effect of the main four parameters that contribute to generating the CP is investigated. Two of them are in the feed line side of the antenna namely the width of the horizontal feeding stub (w_t) and the radius of the circular patch (R) that terminates the vertical feeding stub. On the ground plane side, the other two investigated parameters are the separation distance between the two rectangular ground stubs (d) and the width of each rectangular ground stub (w_s).

Figure 8 shows the reflection coefficient and axial ratio of the proposed wide-slot antenna at different values of w_t keeping $R = 1.5mm$, $w_s = 2mm$, and $d = 6.3mm$. This parameter has no effect on the -10dB impedance BW of the antenna because it just tunes the coupling between the feed line and the square radiating stub, so it only modifies the matching at the resonant frequency. However, it has a direct influence on the location of the 3dB ARBW because it controls the location of the first current entrance to the square radiating slot as explained in the previous section. The value $w_t = 12\ mm$ gives the best location for the feeding point so that the 3dB ARBW perfectly covers LTE 42 and LTE 43 standards.

As demonstrated in Section III, the vertical feeding stub which is ended with a circular patch provides a coupling with the rectangular ground stubs, and it slightly modifies their

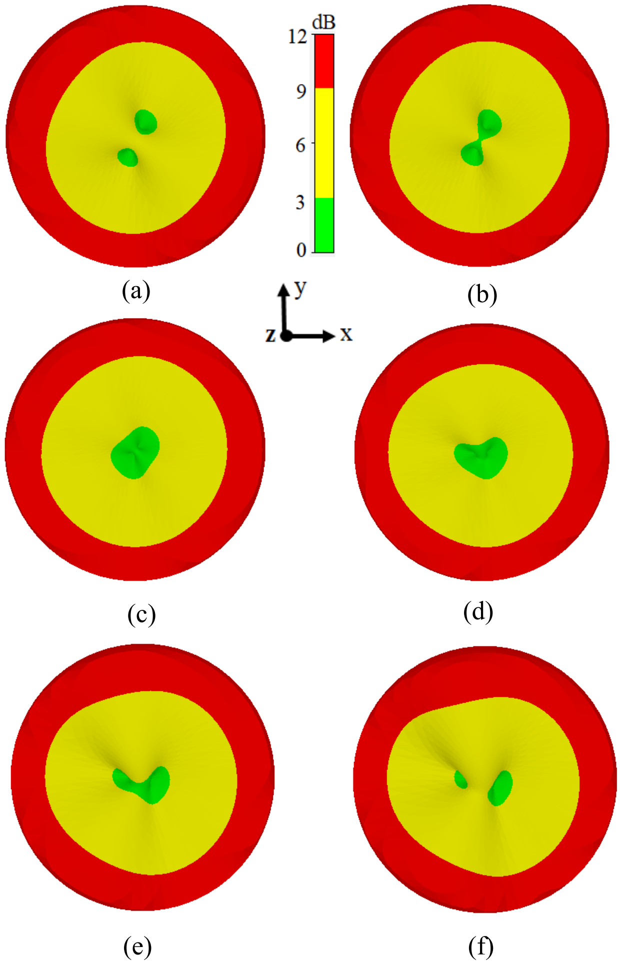

FIGURE 6. The 3D axial ratio pattern of the wide-slot antenna at (a) f=3.36 GHz, (b) f=3.38 GHz, (c) f=3.55 GHz, (d) f=3.75 GHz, (e) f=3.87 GHz, and (f) f=3.95 GHz.

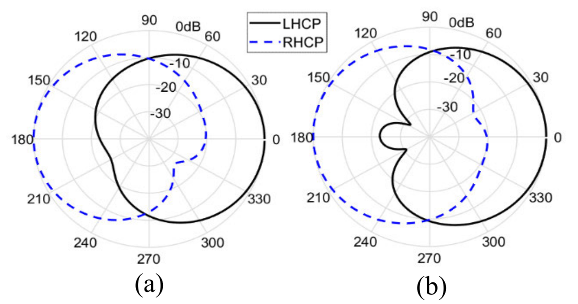

FIGURE 7. Simulated left hand and right hand circular polarization radiation patterns at f=3.55 GHz (a) yz-plane and (b) xz-plane.MEASURED RESULTS.

electrical length. Therefore, varying the radius R results in controlling the position of the antenna resonant frequency and the 3dB ARBW of the antenna because this parameter affects the second path of the current that feeds the square radiating slot as shown in Figure 9. A radius $R = 1.5\ mm$ represents the best value that provides -10dB impedance BW and 3dB ARBW that extend along the intended 5G mid-band standards.

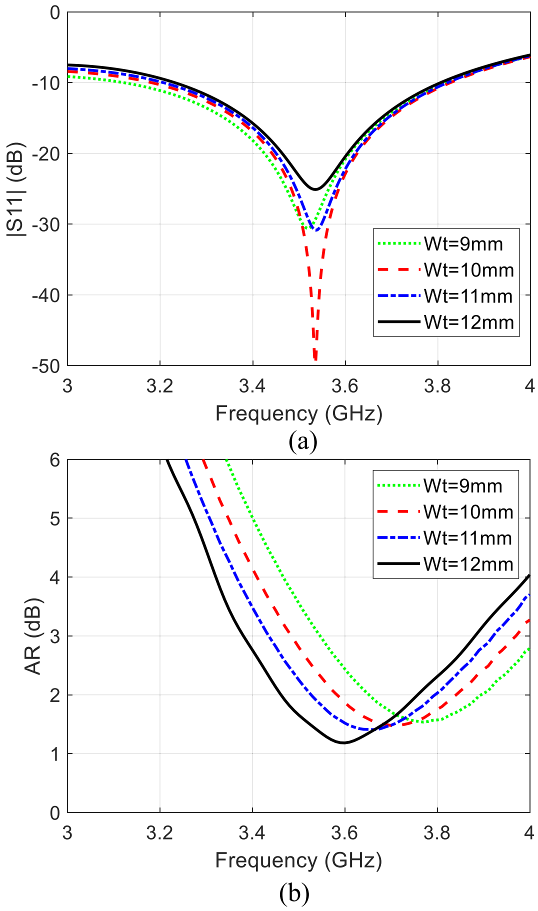

FIGURE 8. **Simulation results of the proposed wide-slot antenna (a) reflection coefficient and (b) axial ratio at $R = 1.5mm$, $w_s = 2mm$, $d = 6.3mm$, and different values of w_t.**

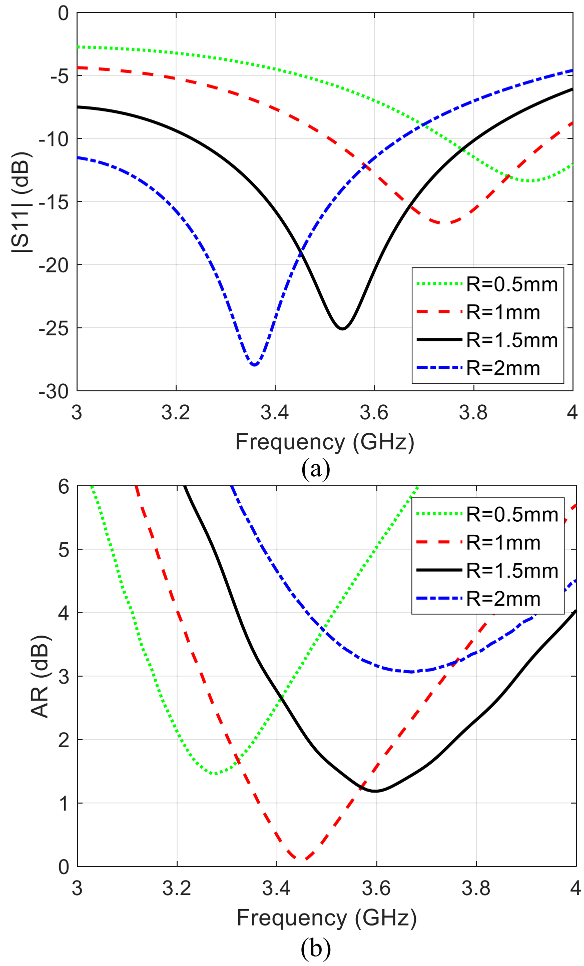

FIGURE 9. **Simulation results of the proposed wide-slot antenna (a) reflection coefficient and (b) axial ratio at $w_t = 12mm$, $w_s = 2mm$, $d = 6.3mm$, and different values of R.**

The same interpretation can be recalled when varying the separation between the rectangular ground stubs (d). As illustrated in Figure 10, the current path of the upper feeding point is modified by this separation as well as the coupling between the feed line and the radiating slot. These modifications result in manipulating the position of the resonant frequency and the 3dB ARBW. Decreasing d leads to a lower resonant frequency since it results in a longer electrical current path. The separation value $d = 6.3\ mm$ generates -10dB BW and ARBW compatible with 5G mid-band applications.

The effect of the width of the rectangular ground stubs w_s on the reflection coefficient and the broad side AR of the proposed wide-slot antenna is illustrated in Figure 11. With respect to the upper feeding point, controlling this parameter is equivalent to controlling the width of a feed line of an antenna which directly manipulates the value of the characteristic impedance. Therefore, the effect of w_s appears as an improvement in the matching at the resonant frequency as well as a fine-tuning for the 3dB ARBW which is located at the range 3.38-3.87 GHz when $w_s = 2\ mm$.

VI. MEASURED RESULTS

The front and back views of the fabricated version of the proposed wide-slot antenna are shown in Figure 12. The measured reflection coefficient is acquired with the aid of Amitec VNA40, and the setup of the measurement is exhibited in Figure 13(a). On the other hand, the gain, radiation pattern, and broadside axial ratio measurement setup are revealed in Figure 13(b).

Figure 14(a) illustrates the simulated and measured reflection coefficients, while Figure 14(b) shows the simulated and measured broad side axial ratio. It is clear that the simulated -10 dB impedance BW is equal to 590 MHz (16.7%) extending along the frequency range (3.23-3.82) GHz, whereas the measured impedance BW is equal to 580 MHz (16.2%) covering the frequency range (3.3-3.88) GHz. The simulated 3dB ARBW is equal to 490 MHz (13.5%) along the range (3.38-3.87) GHz, while the measured 3dB ARBW is found to be 440 MHz (12.2%) over the frequency range (3.4-3.84) GHz. The measured and simulated impedance BW and ARBW values perfectly cover the LTE 42 and LTE

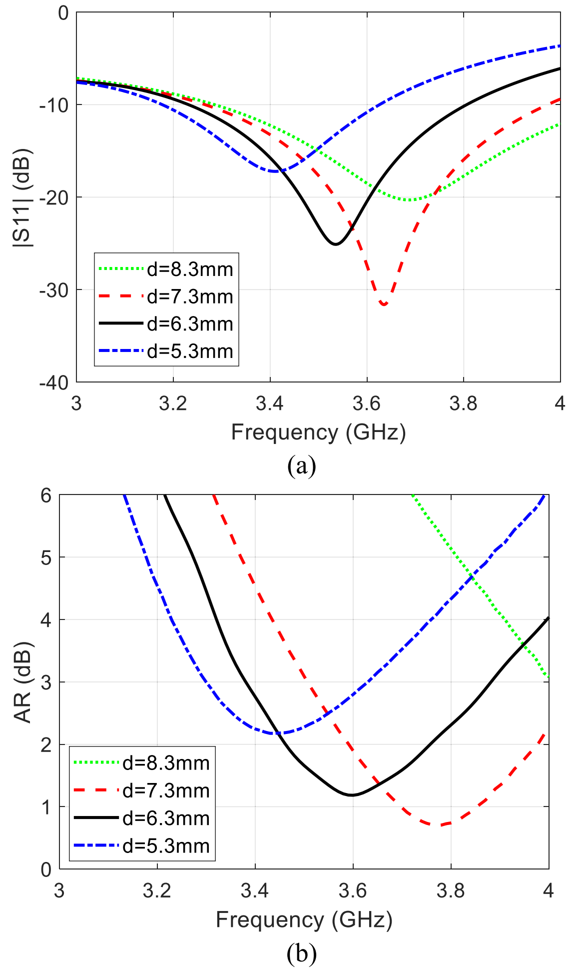

FIGURE 10. Simulation results of the proposed wide-slot antenna (a) reflection coefficient and (b) axial ratio at $w_t = 12mm$, $w_s = 2mm$, $R = 1.5mm$, and different values of d.

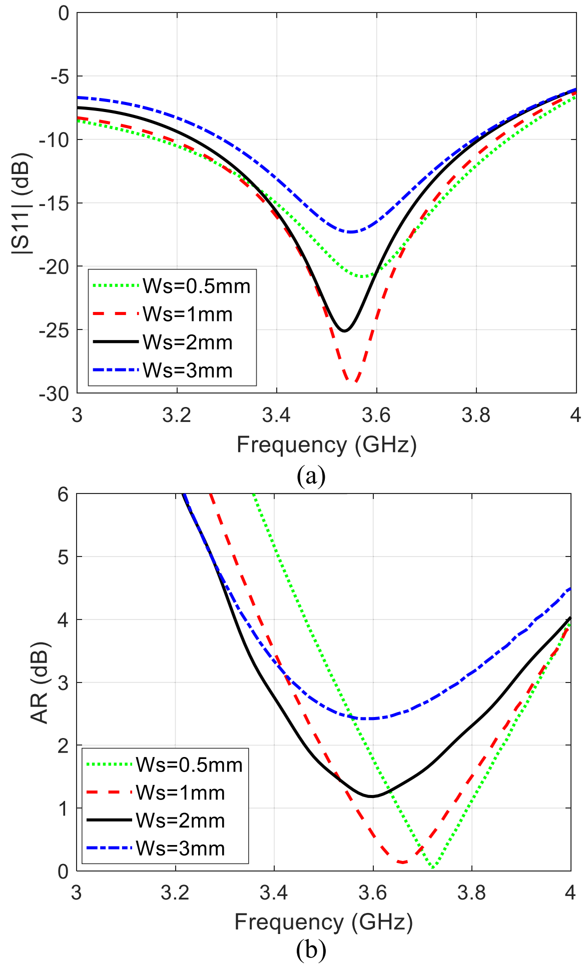

FIGURE 11. Simulation results of the proposed wide-slot antenna (a) reflection coefficient and (b) axial ratio at $w_t = 12mm$, $d = 6.3mm$, $R = 1.5mm$, and different values of w_s.

43 standards of the 5G mid-band applications. The deviation between the simulated and measured results may be attributed to many factors such as the imperfect solder of the SMA connector, the imperfection of the fabrication process, and irregular variation of the dielectric constant of the substrate along the operational frequency band.

The simulated and measured gains are illustrated in Figure 15. The simulated and measured gain values are larger than 2.5 dBi along the frequency range of the LTE 42 and LTE 43. The measured gain has values less than the simulated gain because of the losses of the imperfect soldering of the SMA connector as well as the reflections that come from the equipment inside the anechoic chamber. However, at frequencies larger than 3.6 GHz, the measured gain values are higher than the simulated ones. The reason behind this is given previously in Figure 14(a). The measured reflection coefficient has values less than the simulated one for frequencies above 3.6 GHz, so the measured realized gain appears with higher values than the simulated realized gain.

Finally, to experimentally verify the presence of the CP in the broad side direction, the simulated co-polarized and cross-polarized radiation patterns at 3.55 GHz are shown in Figure 16. The co- and cross-polarized patterns are close to each other (with a difference of less than 3dB) in the broadside direction ($\theta = 0°$), and this is good evidence for the presence of the CP in that direction.

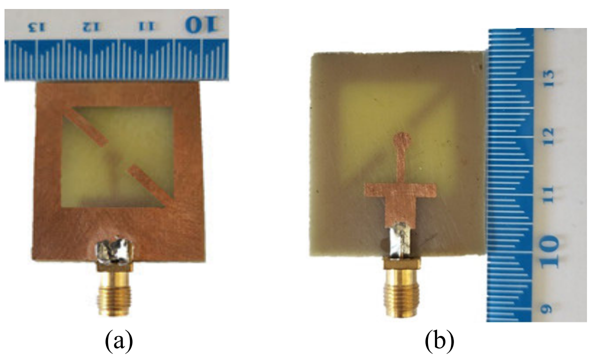

FIGURE 12. The fabricated wide-slot antenna (a) front view and (b) back view.

In general, the 5G antenna designers propose antennas for 5G mid-band either in the LTE 43 standard [23], [24]

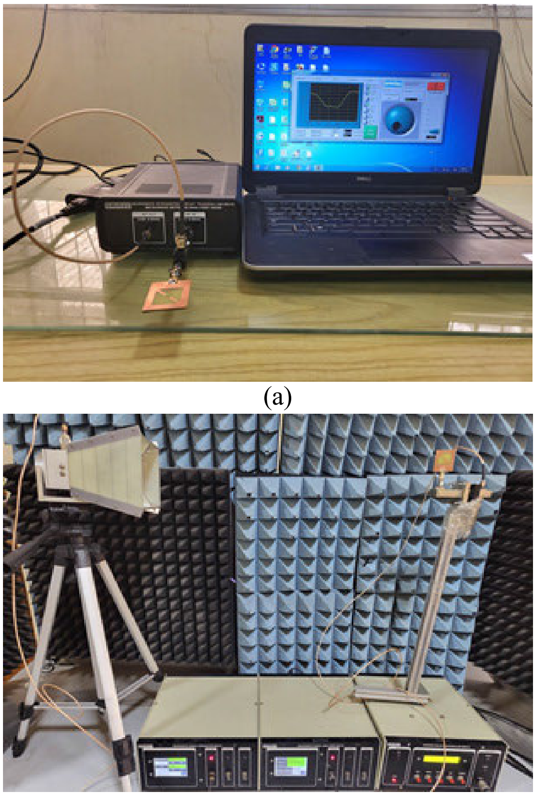

(a)

(b)

FIGURE 13. The measurements set up (a) S_{11} measurements and (b) radiation pattern, axial ration, and gain measurements.

TABLE 1. Comparison between the proposed antenna and other designs.

Ref.	Ant. Dimensions in λₒ	-10 dB BW %	3 dB ARBW %	Gain dB
[10]	0.48 × 0.58 × 0.03	13.8	4.5	3
[11]	0.54 × 0.94 × 0.03	7	1.5	5.34
[12]	0.55 × 0.91 × 0.03	4.2	2.14	2.85
[13]	0.54 × 0.94 × 0.03	15.6	7.05	3.9
[16]	0.44 × 0.97 × 0.03	12.4	6.25	6
[17]	0.36 × 0.36 × 0.04	10.9	4.12	3.1
[27]	2.72 × 3.06 × 0.917	5.6	5	1.6
[28]	0.85 × 0.85 × 0.16	19.15	12.6	6
[29]	1.04 × 0.74 × 0.07	19.6	9.2	8.25
[30]	0.334 × 0.334 × 0.019	13.8	4.65	3
Proposed	0.41 × 0.36 × 0.02	16.2	12.2	3.1

or in the LTE 42 standard [25], [26]. Unfortunately, these designs cannot be used in devices that works on the two standards because this requires using two different antennas for each standard. This drawback is solved in this work by proposing antenna that works on these two standards. Table 1 gives a comparison between the proposed design and some other important CP antennas. Since the listed antennas are operating at different frequency bands, the dimensions of them are given in terms of their resonant wavelengths rather than in (mm). This is necessary to present a fair comparison

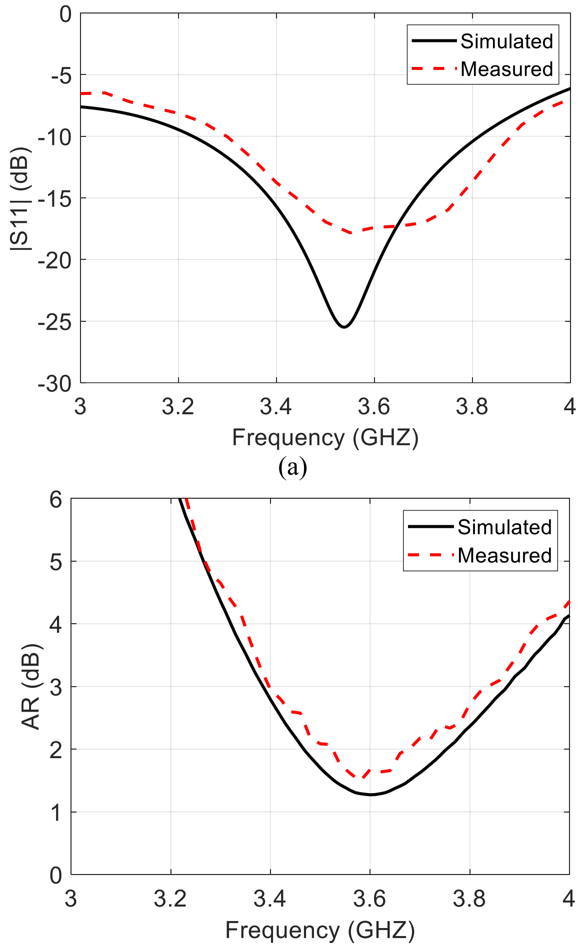

(a)

(b)

FIGURE 14. Simulated and measured results of the proposed wide-slot antenna (a) reflection coefficient and (b) axial ratio.

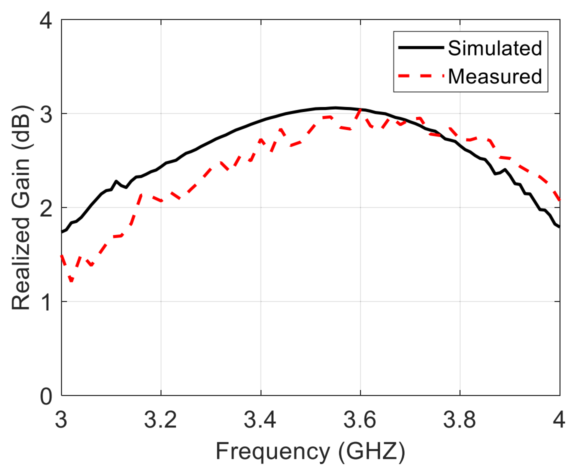

FIGURE 15. Simulated and measured realized gains of the proposed wide-slot antenna.

between them, where λ_o represents the freespace wavelength corresponding to the first resonant frequency of the antenna. The table shows that in spite of the antenna compact size, it makes good balance between the BW, ARBW, and gain as

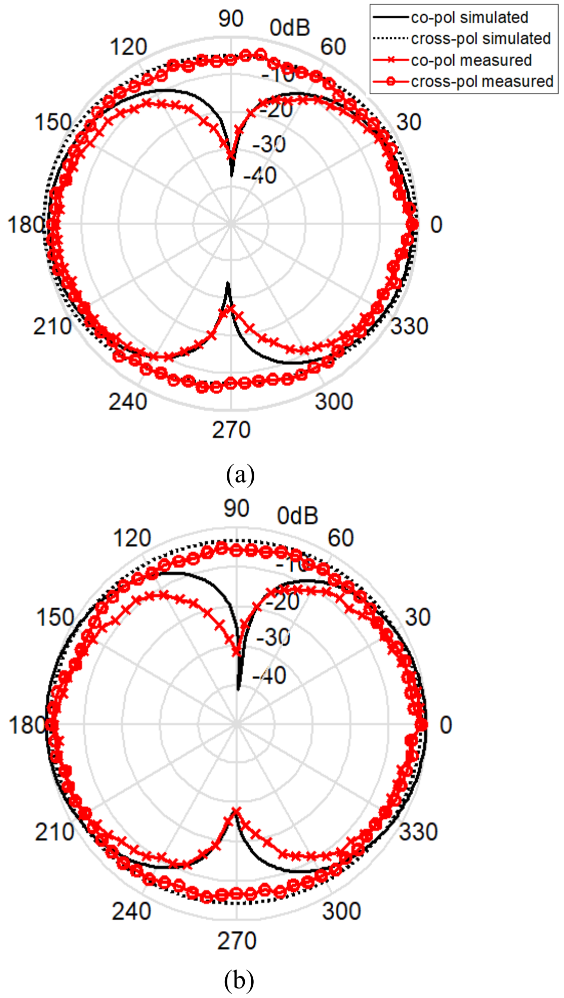

FIGURE 16. **The co-polarized and cross-polarized radiation patterns of the proposed antenna at f=3.55 GHz (a) yz-plane and (b) xz-plane.**

well as its perfect coverage for the 5G mid-band standards. Additional single element CP antennas [27], [28], [29], [30] are also listed in the below table.

It is worth to mention that some of the references used in the comparison are MIMO antennas. However, the table compares the size and the performance of the proposed antenna with a single element of the MIMO structure because the CP is generated by a single element. The MIMO structure is either used for spatial diversity or beamforming purposes only, and it does not contribute in the generation of the CP.

VII. CONCLUSION

A compact wide-slot antenna with broadband LHCP coverage suitable for 5G mid-band applications has been proposed in this work. The mechanism that led to obtain the CP in the broadside direction of the antenna has been demonstrated in detail. In spite of the antenna compact size ($0.41\lambda_o \times 0.36\lambda_o \times 0.02\lambda_o$), the antenna has measured impedance BW equal to 16.2% (3.38-3.87) GHz and ARBW equal to 12.2% (3.4-3.84) GHz that perfectly encompasses the two widely used standards (LTE 42 and LTE 43) of the 5G mid-band. The antenna also has very acceptable gain values that exceed 2.5 dB over the entire operational band. As a future work, a MIMO version of the proposed wide-slot antenna will be designed to be more compatible with the handsets of mobile communication systems.

REFERENCES

[1] K.-L. Wong, *Compact and Broadband Microstrip Antennas* (Wiley Series in Microwave and Optical Engineering). New York, NY, USA: Wiley, 2002.
[2] C. A. Balanis, *Antenna Theory: Analysis and Design*. Hoboken, NJ, USA: Wiley, 2016.
[3] N. Evans, Y. Liu, L. Shafai, and D. Isleifson, "Capacitively coupled single-layer dual-band circularly polarized GPS ring antennas," in *Proc. IEEE 19th Int. Symp. Antenna Technol. Appl. Electromagn. (ANTEM)*, Aug. 2021, pp. 1–2.
[4] E. Zhang, A. Michel, P. Nepa, and J. Qiu, "Multifeed tri-band circularly polarized antenna for UHF/MW-RFID application," *Int. J. RF Microw. Comput.-Aided Eng.*, vol. 32, no. 1, Jan. 2022, Art. no. e22939.
[5] I. Fatima, A. Ahmad, S. Ali, M. Ali, and M. I. Baig, "Triple-band circular polarized antenna for WLAN/Wi-Fi/Bluetooth/WiMAX applications," *Prog. Electromagn. Res. C*, vol. 109, pp. 65–75, 2021.
[6] M. F. Farooqui and A. Kishk, "3-D-printed tunable circularly polarized microstrip patch antenna," *IEEE Antennas Wireless Propag. Lett.*, vol. 18, no. 7, pp. 1429–1432, Jul. 2019.
[7] Y. Liu, S. Cai, X. Xiong, W. Li, and J. Yang, "A novel wideband circularly polarized modified square-slot antenna with loaded strips," *Int. J. RF Microw. Comput.-Aided Eng.*, vol. 29, no. 10, Oct. 2019, Art. no. e21873.
[8] L. Hao, C. Fan, H. Wang, B. Li, and W. Yin, "Novel square slot circularly polarized antenna with broadband characteristics," *Int. J. RF Microw. Comput.-Aided Eng.*, vol. 32, no. 1, Jan. 2022, Art. no. e22921.
[9] F. M. Alnahwi, Y. I. A. Al-Yasir, N. T. Ali, I. Gharbia, C. H. See, and R. A. Abd-Alhameed, "A compact wideband circularly polarized planar monopole antenna with axial ratio bandwidth entirely encompassing the antenna bandwidth," *IEEE Access*, vol. 10, pp. 81828–81835, 2022.
[10] J. Malik, A. Patnaik, and M. Kartikeyan, "Novel printed MIMO antenna with pattern and polarization diversity," *IEEE Antennas Wireless Propag. Lett.*, vol. 14, pp. 739–742, 2015.
[11] L. Malviya, R. K. Panigrahi, and M. V. Kartikeyan, "Circularly polarized 2 × 2 MIMO antenna for WLAN applications," *Prog. Electromagn. Res. C*, vol. 66, pp. 97–107, 2016.
[12] Y. Sharma, D. Sarkar, K. Saurav, and K. V. Srivastava, "Three-element MIMO antenna system with pattern and polarization diversity for WLAN applications," *IEEE Antennas Wireless Propag. Lett.*, vol. 16, pp. 1163–1166, 2017.
[13] N. K. Sahu, G. Das, and R. K. Gangwar, "L-shaped dielectric resonator based circularly polarized multi-input-multi-output (MIMO) antenna for wireless local area network (WLAN) applications," *Int. J. RF Microw. Comput.-Aided Eng.*, vol. 28, no. 9, Nov. 2018, Art. no. e21426.
[14] G. Varshney, R. Singh, V. S. Pandey, and R. S. Yaduvanshi, "Circularly polarized two-port MIMO dielectric resonator antenna," *Prog. Electromagn. Res. M*, vol. 91, pp. 19–28, 2020.
[15] S.-D. Xu, D.-F. Guan, L. Liu, Q. Zhang, H. Xu, and S.-W. Yong, "A narrow-band circularly polarized leaky-wave antenna with open stopband suppressed," *Int. J. RF Microw. Comput.-Aided Eng.*, vol. 31, no. 7, 2021, Art. no. e22647.
[16] I. Khan, Q. Wu, I. Ullah, S. U. Rahman, H. Ullah, and K. Zhang, "Designed circularly polarized two-port microstrip MIMO antenna for WLAN applications," *Appl. Sci.*, vol. 12, no. 3, p. 1068, Jan. 2022.
[17] F. M. Alnahwi, Y. I. A. Al-Yasir, C. H. See, and R. A. Abd-Alhameed, "Single-element and MIMO circularly polarized microstrip antennas with negligible back radiation for 5G mid-band handsets," *Sensors*, vol. 22, no. 8, p. 3067, Apr. 2022.
[18] Y. Sung, "Bandwidth enhancement of a microstrip line-fed printed wide-slot antenna with a parasitic center patch," *IEEE Trans. Antennas Propag.*, vol. 60, no. 4, pp. 1712–1716, Apr. 2012.
[19] F. M. Alnahwi and N. E. Islam, "A generalized concept for band notch generation in ultra-wide band antennas," *Prog. Electromagn. Res. C*, vol. 54, pp. 179–185, 2014.

[20] *3D EM Simulation Software*, CST Studio Suite, Bradford Univ., 2021.
[21] A. K. Dwivedi, A. Sharma, A. K. Pandey, and V. Singh, "Two port circularly polarized MIMO antenna design and investigation for 5G communication systems," *Wireless Pers. Commun.*, vol. 120, no. 3, pp. 2085–2099, Oct. 2021.
[22] A. K. Dwivedi, A. Sharma, A. K. Singh, and V. Singh, "Circularly polarized two port MIMO cylindrical DRA for 5G applications," Presented at the Int. Conf. U.K.-China Emerg. Technol. (UCET), 2020.
[23] F. K. Juma'a, A. I. Al-Mayoof, A. A. Abdulhameed, F. M. Alnahwi, Y. I. A. Al-Yasir, and R. A. Abd-Alhameed, "Design and implementation of a miniaturized filtering antenna for 5G mid-band applications," *Electronics*, vol. 11, no. 19, p. 2979, Sep. 2022.
[24] F. T. Çelik, L. Alatan, and Ö. A. Çivi, "A pattern reconfigurable compact antenna structure based on shorted microstrip patches," Presented at the 16th Eur. Conf. Antennas Propag. (EuCAP), 2022.
[25] S. Hu, Y. Hu, H. Zheng, W. Zhu, Y. Gao, and X. Zhang, "A compact 3.3–3.5 GHz filter based on modified composite right-/left-handed resonator units," *Electronics*, vol. 9, no. 1, p. 1, Dec. 2019.
[26] Y. N. Rahmawati, H. Ludiyati and S. Sardjito, "The characteristic of a 3.5 GHz circular patch antenna using open-ring artificial dielectric," in *Proc. 2nd Int. Seminar Sci. Appl. Technol. (ISSAT)*, 2021, pp. 387–393.
[27] C. Turkmen and M. Secmen, "Bandwidth enhancement of omnidirectional circularly polarized Slotted antenna for satellite communication," in *Proc. 32th Int. Union Radio Sci. Gen. Assem. Sci. Symp.*, 2017, pp. 1–4.
[28] Y. Yu, D. Hong, M.-C. Tang, D. Yi, and M. Li, "A compact near-field resonant parasitic slot helix antenna with wide axial ratio bandwidth," *IEEE Antennas Wireless Propag. Lett.*, early access, Oct. 19, 2022, doi: 10.1109/LAWP.2022.3215860.
[29] M. Hussain, S. Abbas, M. Alibakhshikenari, M. Dalarsson, and F. Falcone, "Circularly polarized wideband antenna for 5G millimeter wave application," in *Proc. IEEE Int. Symp. Antennas Propag. USNC-URSI Radio Sci. Meeting (AP-S/URSI)*, Jul. 2022, pp. 830–831.
[30] F. M. Alnahwi, H. L. Swadi, and A. S. Abdullah, "Design and simulation of single and 2×2 MIMO circularly polarized patch antennas with a pair of chip resistors for 5G applications," in *Proc. Int. Symp. Multidisciplinary Stud. Innov. Technol. (ISMSIT)*, 2022, pp. 488–493, doi: 10.1109/ISMSIT56059.2022.9932653.

FALIH M. ALNAHWI received the B.Sc. and M.Sc. degrees from the University of Basrah, Iraq, in 2004 and 2007, respectively, and the Ph.D. degree in electrical and computer engineering from the University of Missouri-Columbia, USA, in 2015. He joined as a Lecturer at the Department of Electrical Engineering, University of Basrah, where he is currently an Associate Professor and the Director of graduate students. His research interests include antennas and wireless propagation especially the multiband, broadband, ultra-wide band antennas, electromagnetic fields, MIMO systems, metamaterial, mutual coupling reduction techniques, reconfigurable antennas, microwave filters design, digital communications, optimization, and electromagnetic compatibility.

YASIR I. A. AL-YASIR (Member, IEEE) received the B.Sc. and M.Sc. degrees from the University of Basrah, Iraq, in 2012 and 2015, respectively, and the Ph.D. degree from the University of Bradford, U.K., in 2021. In 2014, he joined as a Research Visitor at the Antennas and RF Engineering Research Group, University of Bradford. From 2018 to 2020, he was appointed at the University of Bradford as a Marie Curie Research Fellow in the H2020-ITN-SECRET Project funded by EU Commission, targeting 5G mobile small cells. He is currently a Staff Member with the Faculty of Engineering and Informatics, University of Bradford, working as a Research Fellow in the SATNEX-V Project, funded by the European Space Agency. He is also a Reviewer for various high-ranking journals and publishers such as IEEE, IET, Wiley, Springer, Elsevier, and MDPI. He has authored two books and ten book chapters and published more than 130 journal and conference papers on aspects of RF and Microwave Engineering. His articles have more than 2044 citations with 24 h-index, reported by the Google Scholar. He was a recipient and co-recipient of various awards and prizes, such as the Best Paper Award from the IEEE 2nd 5G World Forum and IEEE 4th 5G Summit Dresden, Germany.

NAZAR T. ALI (Senior Member, IEEE) received the Ph.D. degree in electrical and electronic engineering from the University of Bradford, U.K., in 1990. From 1990 to 2000, he held various posts at the University of Bradford as a Researcher and Lecturer. He worked in many collaborative research projects in the U.K. under the umbrella of the Centre of Research Excellence, Department of Trade and Industry (DTI) and EPSERC. This involved a consortium of a number of universities and industrial companies. He is currently an Associate Professor with Khalifa University, United Arab Emirates. He has over 100 articles published in peer reviewed high quality journals and conferences. His current research interests include antennas and RF circuits and systems, indoor and outdoor localization techniques, and RF measurements.

IBRAHIM GHARBIA received the B.Sc. degree in electrical and electronic engineering from the Department of Electrical and Electronic Engineering, Subrata Engineering Faculty, Libya, in 1997, and the M.Sc. degree from the University of Huddersfield, U.K., in 2012. He is currently pursuing the doctoral degree with the Radio Frequency Research Group, Bradford University. He was a Lecturer of computing, science, and mathematics and a Research Assistant at the Libyan Forensic Laboratory, where he was recognised as the Best Employee in his department. Training Courses supporting the Digital Evidence Forensic Science were actively pursued at Huddersfield University by the student, from 2012 to 2015. From 2006 to May 2012, he was at the Catholic Housing Aid Society, from 2015 to 2018, he was an Interpreter at Bradford, and was the Chairperson at the New Libya Society. His research interests include RFID reader and tag designs, programming, sensor design, antenna design, electromagnetic fields, and MIMO. He received the scholarship for his M.Sc. degree.

ABDULKAREEM S. ABDULLAH (Senior Member, IEEE) received the B.Sc. and M.Sc. degrees in communication engineering from the College of Engineering, University of Basrah, in 1980 and 1985, respectively, the Ph.D. degree in electromagnetic fields and microwaves technology from the Beijing University of Posts and Telecommunications (BUPT), Beijing, China, in 2004, and the postdoctoral degree in telecommunications engineering from the Beijing Institute of Technology, China, in 2008.

He is currently working as a Professor with the Department of Electrical Engineering, College of Engineering, University of Basrah. He has published more than 100 journal and conference papers. His research interests include antenna design and analysis, smart antennas, microwaves technology, and indoor and outdoor radio waves propagation.

YIM FUN HU (Senior Member, IEEE) received the B.Sc. degree (Hons.) in mathematical sciences and the Ph.D. degree in information systems engineering from the University of Bradford, Bradford, U.K., in 1984 and 1987, respectively. She was the Head of the Department of Biomedical and Electronics Engineering, Faculty of Engineering and Informatics. She is a Professor of wireless communication engineering and the Director of the Bradford-Renduchintala Centre for Space AI, Faculty of Engineering and Informatics, University of Bradford. She has published over 150 journal and conference papers and coauthored two books and several book chapters. Her research interests include mobile, wireless, and satellite communication networking, including software-defined networking, network function virtualization, mobility management, radio resource management, and network management in 5G networks, applying her research expertise to more than 15 EU and ESA flagship projects in mobile, satellite, aeronautical communications, and fast speed trains as well as many other national, international, and industrial funded projects. She is a fellow of the Institution of Engineering and Technology. She was a recipient of the U.K. Yorkshire Forward Chair of wireless communications engineering.

RAED A. ABD-ALHAMEED (Senior Member, IEEE) is currently a Professor of electromagnetic and radiofrequency engineering with the University of Bradford, U.K. He is also the Leader of radiofrequency, propagation, sensor design, and signal processing; in addition to leading the Communications Research Group for years within the School of Engineering and Informatics, University of Bradford. He has long years of research experience in the areas of radio frequency, signal processing, propagations, antennas, and electromagnetic computational techniques. He has been a Professor Research Visitor of Wrexham University, Wales, since 2009, covering the wireless and communications research areas. He has published over 800 academic journals and conference papers, coauthored eight books and several book chapters, and seven patents. He is a Principal Investigator for several funded applications to EPSRCs, Innovate U.K., British Council, and the Leader of several successful knowledge Transfer Programmes, such as with Arris (previously known as Pace plc), Yorkshire Water plc, Harvard Engineering plc, IETG Ltd., Seven Technologies Group, Emkay Ltd., and Two World Ltd. He has also been a co-investigator in several funded research projects, including Horizon Research and Innovation MSCA-RISE-Robust 2022-2027, Marie Skłodowska-Curie, titled: Research and Innovation, titled: FractuRe Orthopaedic Rehabilitation: Ubiquitous eHealth Solution; 2) Horizon 2020 Research and Innovation programme under grant agreement H2020-MSCA-RISE-2019-eBORDER-872878; 3) H2020 MARIE Skłodowska-CURIE ACTIONS: Innovative Training Networks Secure Network Coding for Next Generation Mobile Small Cells 5G-US; 4) European Space Agency: Satellite Network of Experts V, Work Item 2.6: Frequency selectivity in phase-only beamformed user terminal direct radiating arrays; 5) Nonlinear and demodulation mechanisms in biological tissue (Department of Health, Mobile Telecommunications and Health Research Programme); and 6) Assessment of the Potential Direct Effects of Cellular Phones on the Nervous System (EU: collaboration with six other major research organizations across Europe). His interests include computational methods and optimizations, wireless and mobile communications, sensor design, EMC, beam steering antennas, Beamforming, energy-efficient PAs, and RF predistorter design applications. He is a fellow of the Institution of Engineering and Technology and a fellow of the Higher Education Academy and a Chartered Engineer. He was a recipient of the Business Innovation Award for his successful Knowledge Transfer Programme with Pace and Datong companies on the design and implementation of MIMO sensor systems and antenna array design for service localizations. He is the Chair of several successful workshops on Energy-Efficient and Reconfigurable Transceivers: Approach toward Energy Conservation and CO_2 Reduction that addresses the biggest challenges for future wireless systems. He has been the General Chair of the IMDC-IST International Conference, since 2020. He has been the Co-Editor of *Electronics* (MDPI) journal, since June 2019. He has been a Guest Editor of *IET Science, Measurements and Technology* journal, since 2009.